Vilnius University
Faculty of Physics
Laser Research Center

Laboratory assignment No. MNFT-1

FABRICATION OF 3D POLYMERIC MICROSTRUCTURES USING PULSED 3D DIRECT LASER LITHOGRAPHY

For master students of Laser Physics and Optical Technologies and Laser Technology programmes

Vilnius 2026

1 Objectives

1. Become familiar with the principle of 3D laser lithography (3DLL) – the photopolymerization technique used in this assignment – and with the construction and operation of the direct laser writing (DLW) system on which it is performed.
2. Understand what limits the spatial resolution of the technology, and which laser irradiation and focusing parameters determine it.
3. Gain practical experience in fabricating various microstructures and in characterizing them by scanning electron microscopy (SEM).

2 Tasks

1. Employing 3DLL technology, fabricate „resolution bridges“ – a test model for determining spatial resolution.
2. Using a SEM, experimentally evaluate the lateral D and longitudinal L voxel dimensions and their dependence on the laser irradiation intensity and on the sample translation velocity.
3. Calculate the voxel aspect ratio L/D and compare the measured dependences with the theoretical model.
4. Fabricate various 2D and 3D microstructures.

3 Questions for the defence

1. Steps of the photopolymerization reaction.
2. A typical optical setup for 3D laser lithography: its main components and their purpose.
3. Typical parameters of the laser irradiation used to induce the photopolymerization reaction.
4. Lateral D and longitudinal L voxel dimensions, the voxel aspect ratio L/D, and their dependence on the numerical aperture of the objective, the laser wavelength, the irradiation intensity and the sample translation velocity.
5. Evaluation methods for the lateral D and longitudinal L voxel dimensions.
6. Principles of scanning electron microscopy.
7. Types and examples of photopolymers used in 3D laser lithography technology.
8. Application fields of the 3D laser lithography technology.

4 Equipment and materials

During the laboratory assignment a DLW system with the femtosecond laser "Pharos" will be used. A sputter coater (Q150R S, *Quorum Technologies*) and a scanning electron microscope (TM-1000, *Hitachi*) are used for the characterization of the microstructures. Sample preparation requires cover glasses (24×32 mm), the photopolymer SZ2080 with the photoinitiator BIS (4,4′-bis(diethylamino)benzophenone, 1 %), the solvent 4-methyl-2-pentanone and immersion oil.

Other laboratory supplies: laboratory glassware, pipettes, tweezers, a sample heating oven, disposable gloves and safety goggles.

The generalized 3DLL scheme is depicted in Fig. 1. The main component of the system is a femtosecond solid-state laser "Pharos" (*Light Conversion, Lithuania*). The active medium is an Yb:KGW crystal, and the central wavelength of the fundamental radiation is $\lambda_f = 1030$ nm. The laser generates pulses of $\tau_L < 300$ fs duration. The pulse repetition rate f can be adjusted in the range of 1–200 kHz. The experiments are performed using the fundamental radiation ($\lambda_f = 1030$ nm), which is directed straight to the focusing objective. If the second harmonic ($\lambda_{IIh} = 515$ nm) is required instead, the removable mirrors RM_1 and RM_2 are inserted into the beam path. They guide the beam into a separate arm of the optical system, where it passes through the nonlinear crystal *NC* and is frequency-doubled; the green arm of the scheme is used only in that case.

The average power of the laser used to expose the photopolymers is set by a two-stage attenuator. The first stage, Attn 1, consisting of a manually rotated $\lambda/2$ phase plate and a Brewster angle polarizer, is used to set the approximate average power of the beam entering the optical system. The second stage, Attn 2, consisting of a $\lambda/2$ phase plate housed in a computer-controlled rotator and a Brewster angle polarizer, is for precise average power adjustment during laser writing. Power calibration is performed by placing the power meter sensor *PM* in the path of the laser beam. The beam is focused into the volume of the photopolymer with the objective Obj (in this work an $NA = 1.4$, $63\times$ immersion objective and/or an $NA = 0.8$, $20\times$ air objective, *NA* being the numerical aperture). When an immersion objective is used, immersion oil is applied between the objective and the cover glass; its refractive index ($n_{im} = 1.518$) is close to that of the glass ($n_s = 1.52$) and of the photopolymer ($n_f = 1.504$). A $2\times$ beam expander *BE* is installed in the beam path: it widens the beam so that it fills the back aperture of the focusing objective, because only a beam that fills the aperture is focused into a spot as small as the numerical aperture allows. A diode illumination source (*LED*) is installed below the mount that holds the cover glass with the sample, and the process is imaged coaxially through the dichroic mirror *DM* with the *CMOS* camera.

Submicrometric precision positioning tables ANT130-110 (*Aerotech, USA*) with linear motor drives are used for the translation of the structured sample in the XY plane of the laser beam waist. Translation in the Z axis is performed by positioning the focusing objective with an ANT130-60 table. Such a positioning system ensures $+/-75$ nm position repeatability in each axis and allows the samples to be translated at a maximum velocity of 300 mm/s. The "3DPoli" (*Femtika, Lithuania*)

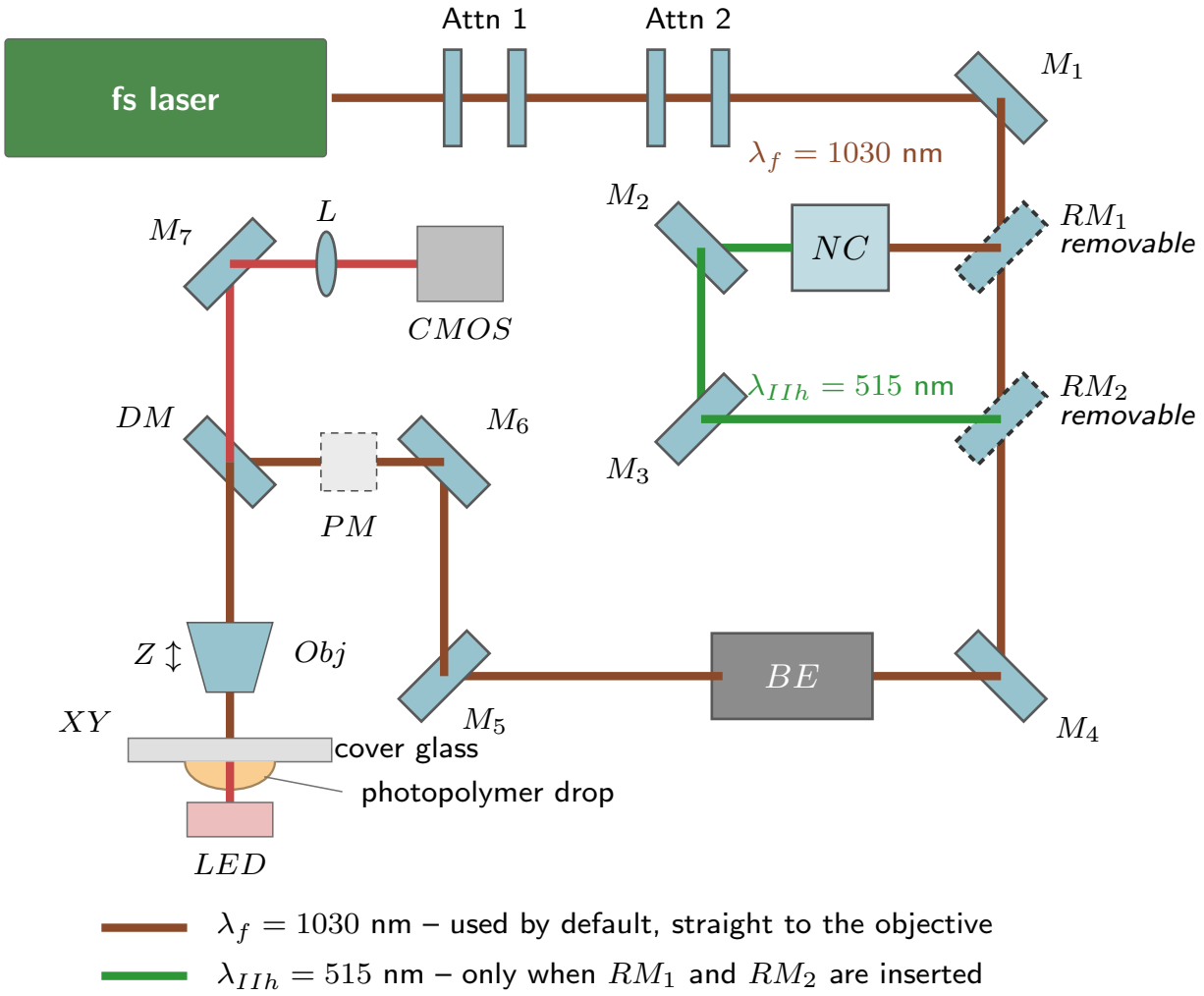


Fig. 1 Generalized scheme of the DLW system; only the main components are shown, and the actual layout may differ. The beam reaches the objective at the fundamental wavelength $\lambda_f = 1030$ nm; the second harmonic $\lambda_{IIh} = 515$ nm is obtained only when the removable mirrors RM_1 and RM_2 are inserted, routing the beam through the nonlinear crystal NC. Meanings of the abbreviations: fs laser – femtosecond laser source, Attn 1, Attn 2 – power attenuator stages, M_1–M_7 – mirrors, RM_1, RM_2 – removable mirrors, NC – nonlinear crystal, BE – beam expander, PM – power meter, DM – dichroic mirror, L – lens, $CMOS$ – camera, Obj – objective, LED – LED illumination source, XYZ – sample translation coordinates.

software package is used to automate the system.

5 Workflow

Before the laboratory assignment, familiarise yourself with the laser safety requirements. In this work you will use a class 4 laser, which means that even scattered radiation can cause eye or skin

injuries if the safety requirements are not fulfilled.

The workflow described below may be adjusted by the instructor depending on the situation in the laboratory. All the fabrication files needed for the assignment will be provided.

1. **Preparation of the material.** The photopolymer SZ2080 + 1 % BIS is drop-cast with a pipette onto two cover glasses: on the first one at the edge of the shorter side – these samples will be used for the „resolution bridges“; on the second one in the middle of the cover glass – these structures will later be used for the molding laboratory assignment (MNFT-2). The samples are then heated in the oven: 1) for 20 min at 40 °C, 2) for 20 min at 70 °C and 3) for 40 min at 90 °C, in order to evaporate the solvent out of the polymer. The oven program P3 is used for this heating step. (NOTE: Due to time constraints, the materials will be prepared in advance by the instructor.) After the heating is complete, the sample is fixed onto the positioning stages with the drop-cast photopolymer facing downward. If an immersion objective is used, a drop of immersion oil is placed on top of the cover glass, directly above the photopolymer droplet on the underside, so that the oil, the glass and the photopolymer lie on the same optical axis; with a non-immersion objective no oil is needed.

2. **Checking the laser system.** Together with the instructor, verify that the system is ready to use: the wavelength (1030 nm), the pulse repetition rate (200 kHz) and the beam alignment.

3. **Computer preparation.**

   (a) Start the *3DPoli Fabrication* and *Compiler* software and the „wxPropView“ camera program used to observe the fabrication process live. The instructor will help with the first launch. For convenience, the camera window is displayed on the auxiliary system monitor.

   (b) In the *3DPoli Fabrication* program, check the fabrication settings: choose the correct parameter file for the objective in use, home all the axes and calibrate the laser power.

4. **Finding the glass–photopolymer interface.** The procedure differs depending on the objective in use.

   With an oil immersion objective. Move the objective towards the sample until its front lens dips into the drop of immersion oil. Then open the laser shutter, set the average power to approximately 5 mW and continue moving the objective downwards in small steps of about 10 µm, watching the camera image:

   (a) burning of the immersion oil is seen – the focal spot is inside the immersion oil;

   (b) bubble formation stops – the focal spot has entered the cover glass;

   (c) after a further 150–170 µm, the thickness of a standard cover glass, microexplosions appear – the focal spot is inside the photopolymer.

Finally, lower the average power to approximately 1 mW – or further still, if microexplosions continue – and locate the interface precisely. Move the objective down in 1 µm steps, and after each step shift the sample 2 µm sideways so that every attempt is made on fresh, unexposed material. The interface has been passed when a polymerized dot appears; as long as no dot appears, the focal spot is still inside the cover glass and the objective has to be moved further down.

With a non-immersion objective. Bring the objective over the photopolymer droplet and set the separation between them to approximately the working distance of the objective. With the laser shutter open and the average laser power set to approximately 5 mW, move the objective in the Z direction in small steps of about 10 µm while watching the camera image, until a polymerization dot or a microexplosion appears – at that moment the focal spot has reached the photopolymer. Then lower the average laser power until microexplosions no longer occur but a polymerized dot is still visible, and locate the interface as described above, moving the objective in 1 µm steps and shifting the sample 5 µm sideways after each step.

5. **Fabrication of the microstructures.**

   (a) Fabricate „resolution bridges“ while changing the average laser power. The power range will be given by the instructor. A typical computer-aided design (CAD) model of „resolution bridges“ is shown in Fig. 2.

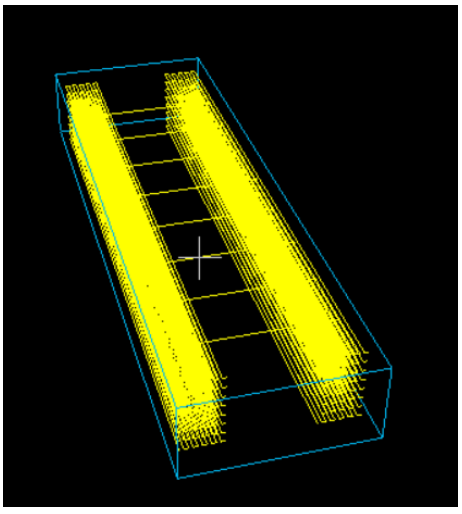


Fig. 2 CAD model of „resolution bridges“.

   (b) Fabricate „resolution bridges“ while changing the sample translation velocity. The velocity range will be given by the instructor.

   (c) Fabricate various microstructures. Examples of CAD models of such objects are shown in Fig. 3. If so instructed, fabricate them on a separate cover glass – these structures will be used in the other laboratory assignments of the course.

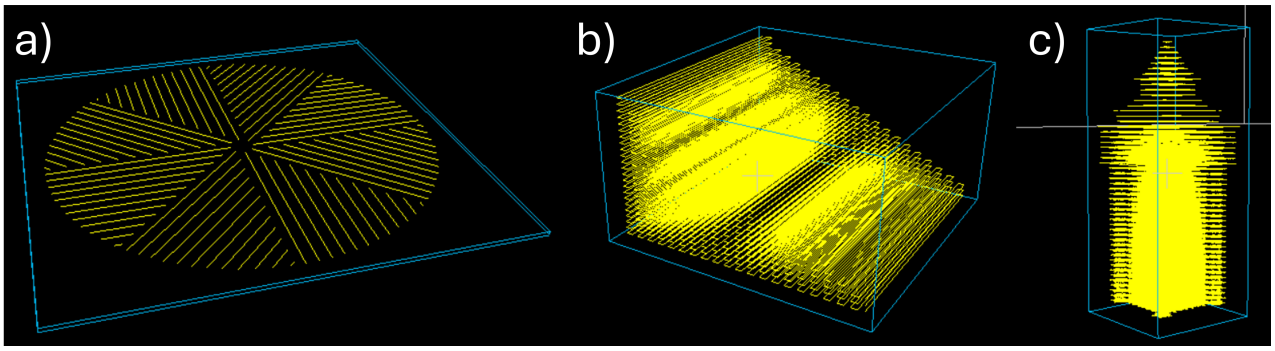


Fig. 3 CAD models of microstructures: a) phase optical element, b) prism, c) tower.

6. **Development.** First clean the immersion oil off the cover glass. Then place the sample in a Coplin jar (or a Petri dish) filled with 4-methyl-2-pentanone for 30 min. Afterwards check whether the photopolymer droplet has been washed away completely. If it has, transfer the sample into another Coplin jar with clean 4-methyl-2-pentanone for 10 min. If it has not, develop it for a further 5 min in the first jar and check again, repeating until the droplet can no longer be seen. Wear gloves when handling the chemicals and work in the fume hood.

7. **Sputter-coating.** The developed and dried sample is coated with 10–20 nm of silver or gold using the sputter coater available in the laboratory (with the assistance of the instructor).

8. **Characterization with a scanning electron microscope.** The whole fabrication and characterization sequence is summarized in Fig. 4. The sample is observed in two positions: top view and angled view (at 45°). Using the microscope software tools, measure the lateral D and longitudinal L voxel dimensions for all the fabricated resolution bridges; remember that the length measured in the tilted view is foreshortened (Section 6.4). NOTE: the manual of the Hitachi TM-1000 microscope is given in the appendix and a paper copy can be found in the laboratory. It is important to read the manual before performing the laboratory assignment.

9. **Plotting the dependence on intensity.** Plot how the lateral and longitudinal voxel dimensions depend on the laser intensity: $f(D,L) \sim I$. The abscissa axis is the intensity (I, TW/cm^2), the ordinate axis the lateral and longitudinal voxel dimensions (D, μm and L, μm). The average laser power is recalculated into intensity according to the formula:

$$I = \frac{2PT}{\pi r_0^2 f \tau_L}; \tag{1}$$

where P – average laser power, T – transmission of the objective, f – pulse repetition rate, r_0 – beam waist radius, τ_L – pulse duration. The beam waist radius is calculated as $r_0 = 0.61M^2\lambda/NA$, where M^2 – beam quality factor, $\lambda = 1030$ nm – the exposure wavelength used in this assignment and NA – the numerical aperture of the objective used.

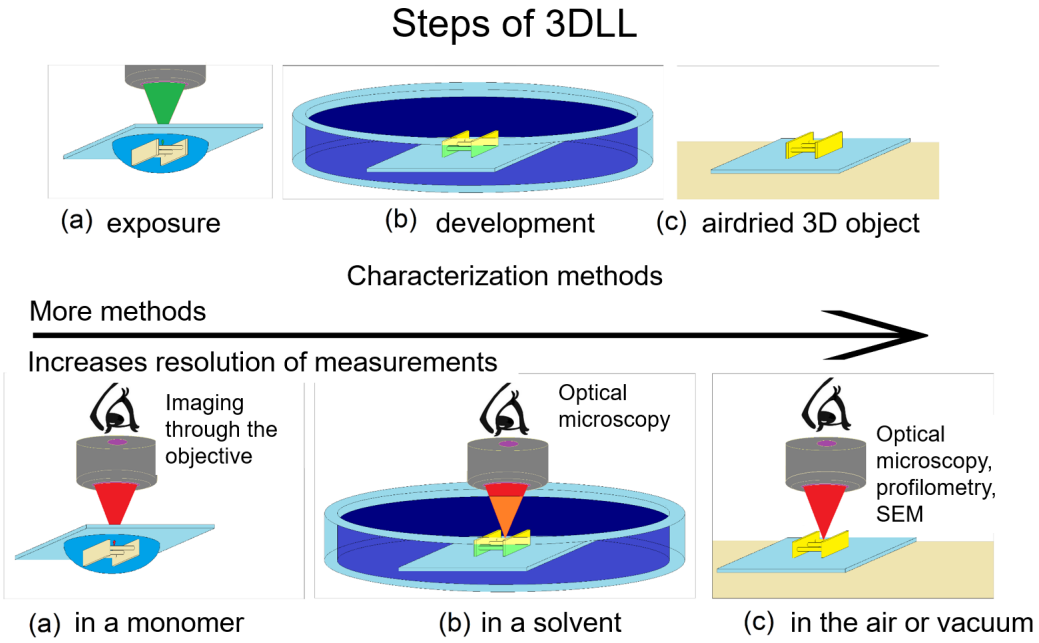


Fig. 4 Scheme of steps of 3DLL fabrication. Characterization methods of the sample at each fabrication step are depicted as well.

10. **Plotting the dependence on translation velocity.** Plot how the lateral and longitudinal voxel dimensions depend on the sample translation velocity: $f(D,L) \sim v$. The abscissa axis is the sample translation velocity (v, µm/s), the ordinate axis the lateral and longitudinal voxel dimensions (D, µm and L, µm).

11. **Aspect ratio and comparison with the theoretical model.** From the same measurements calculate the voxel aspect ratio L/D and plot it against the intensity and against the translation velocity. Compare all the measured dependences with the predictions of Equations 11 and 12 (Fig. 7).

12. **Report and conclusions.** Prepare a report on the assignment. It should state the conditions of the experiment – the objective and its NA, the exposure wavelength, the pulse repetition rate, the pulse duration, and the power and velocity ranges used – and include the relevant SEM images of the fabricated microstructures together with the plots prepared in the previous steps. Discuss the results and write your conclusions.

6 Theory

6.1 Mechanisms of photopolymerization

Polymerization is a chemical reaction in which low molecular weight molecules combine into high molecular weight compounds of identical chemical composition due to external influences to form three-dimensional networks of polymer chains. The connection of a monomer molecule to polymer chains can be initiated using external energy. There are two different mechanisms for this reaction: chain polymerization and step polymerization, the latter also known as photo-crosslinking. The chemical reaction, in which solid polymer networks are formed due to the external effects of light, is called photopolymerization [1].

We will call photopolymers materials consisting of two main components: monomers/oligomers (denoted M) and a photoinitiator (denoted PI). Photoinitiators are materials with low photo-dissociation energy designed to increase the photosensitivity of a mixture. In the case where the external energy source initiating the polymerization reaction is light, the most common polymerization mechanism is based on chain propagation. This mechanism consists of three stages: initiation, propagation, and termination [2, 3]. Initiation begins when a photoinitiator is excited by interaction with light ($PI^\star$) and free radicals are generated ($R^\star$) (Equation 2). Further interaction of these radicals with monomers creates a new molecule with a free bond (Equation 3). As the propagation process begins, successive monomer molecules are attached to the free bond (Equations 4 and 5). During the propagation process, the polymer chain elongates rapidly and the excitation energy is no longer required for this process. The propagation process continues until a free radical is attached to the free bond (Equation 6) or another polymer chain with a free linkage is attached (Equation 7). After such coupling, a chemically inactive polymer chain is obtained [3].

$$PI \xrightarrow{h\nu} PI^\star \rightarrow R^\star \tag{2}$$

$$R^\star + M_1 = RM_1^\star \tag{3}$$

$$RM_1^\star + M_2 = RM_1M_2^\star \tag{4}$$

$$RM_1 \ldots M_n^\star + M_k = RM_{n+k}^\star \tag{5}$$

$$RM_{n+k}^\star + R^\star = RM_{n+k}R \tag{6}$$

$$RM_n^\star + RM_m^\star = RM_nM_mR \tag{7}$$

Compared to other polymerization initiation mechanisms, such as thermal initiation, in which thermal energy creates active polymerization centers, photopolymerization has several important advantages. It is the initiation of polymerization with a light source that enables precise control of the polymerization process both in time and space. Depending on the type and concentration of the photoinitiator, commercially available photopolymers generally have strong absorption in the UV range

and transmittance in the visible and NIR region. This means that the photoinitiator molecule can be excited by absorbing a photon in the UV region or several photons in the IR region. This phenomenon of nonlinear optics is called multiphoton absorption, and the 3DLL method is based on this phenomenon, enabling the formation of 3D objects in a photopolymer volume.

6.2 3D laser lithography

3DLL is a DLW method based on nonlinear absorption of laser irradiation in the photopolymer volume. The two terms are not interchangeable: direct laser writing is the more general one, covering any technique in which a tightly focused beam is translated through a material and modifies it point by point, while 3DLL is the particular case in which that modification is the photopolymerization of a photoresist.

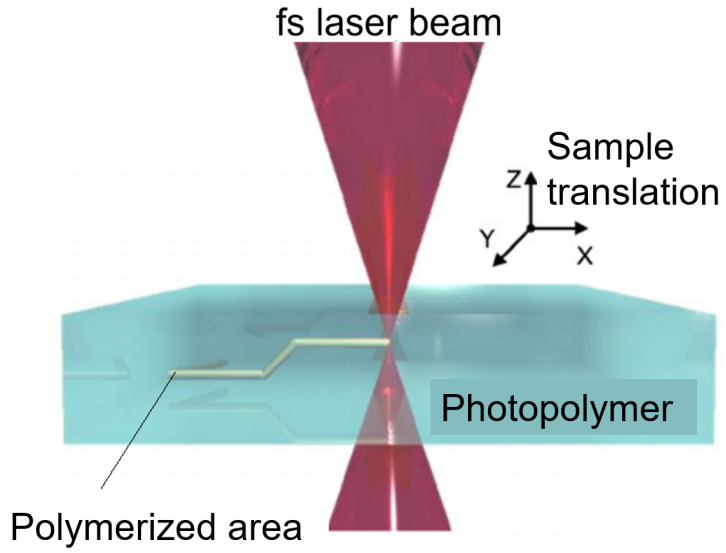


Fig. 5 Structuring of photosensitive material by 3DLL method. Multiphoton absorption and the subsequent polymerization reactions occur only in the waist of the focused beam. Adapted from [4].

Most commercially available photopolymers are optimized for processing by exposure to UV radiation. Such polymers strongly absorb UV radiation, but are relatively transparent to visible and NIR radiation. However, radiation of longer wavelengths can be absorbed by sharply focusing the laser beam and inducing multiphoton absorption in a small volume, which is a nonlinear quantum mechanical process. Multiphoton absorption can be understood as the excitation of an electron through a virtual energy level in a bandgap. It follows from the Heisenberg uncertainty principle that the lifetime of a virtual energy level is very short (several fs) and that the simultaneous absorption of several photons by an electron in the virtual level is a probabilistic event, so multiphoton absorption is a threshold process and occurs only at high (starting with GW/cm^2) irradiation intensity.

The schematic diagram of 3DLL is shown in Fig. 5. Most of the radiation that is focused from above by an objective with a large numerical aperture propagates through the material without interacting with it. The interaction of the exposing light with the material takes place only in a strictly limited volume – the beam waist, where the light intensity reached is sufficient to induce multiphoton absorption. If the sample is translated in three-dimensional space with respect to the laser beam waist, we will polymerize a three-dimensional object, the fidelity of which will depend on the accuracy and resolution of the positioning device, and the smallest structured element will depend on the intensity and focusing conditions (numerical aperture). Material that has not been exposed to focused laser irradiation during structuring will be washed out with the appropriate solvent during development, leaving only the polymerized three-dimensional object [1].

From a technological point of view, 3DLL is performed by exposing the light-sensitive material with a focused beam point by point, following a user-generated CAD model. Three-dimensional exposure of a sample to laser irradiation is accomplished in three ways:

1. In the x and y coordinates, the sample is scanned using a galvanoscanner, and the scan in the z direction is performed by changing the position of the sample itself on stepper or linear translation stages. Scanning with a galvanoscanner is fast, but the field of view is restricted to the area the scanner can address without distorting the focal spot.

2. The position of the laser-focusing objective is fixed at all times, and the structure is formed by translating the sample in the x, y and z directions on the stages mentioned previously. This removes the field-of-view restriction, but the stages are slower than a galvanoscanner.

3. The two movements are combined and synchronized, so that the galvanoscanner writes while the translation stages move at the same time. The beam is then no longer limited to the scanner field, and structures much larger than that field can be written in one piece without stitching errors. This mode is called infinite field of view (IFOV).

Let us also introduce the concept of a polymerization window – it is a ratio $\frac{I_{odt}}{I_{pt}}$, where I_{pt} – the polymerization threshold, the intensity at which the polymerization reaction is initiated, I_{odt} – the optical damage threshold, the intensity at which a bubble forms in the volume of the polymer, in other words, the polymer is optically damaged [1]. Such an analysis is accurate for a polymerization reaction initiated by a single laser pulse. In a real 3DLL experiment, the material is structured at a high repetition rate (of the order of 10^5–10^7 Hz); therefore, it is necessary to take into account the influence of thermoaccumulation phenomena on the change of the process window. When forming 3D structures, the photopolymer is translated in space at a finite velocity v. The number of pulses that reach one point of the material – the pulse overlap – is therefore inversely proportional to that velocity: the faster the sample is moved, the fewer pulses each point receives. Since lasers are used with pulse repetition rates of hundreds of kilohertz, we are dealing not with single pulses or tens of pulses, but with tens of thousands of pulses affecting a local segment of material. Thus, without changing other

parameters, the exposure intensity limits of the polymerization process window will also depend on the translation velocity.

6.3 Spatial resolution: theoretical model and empirical measurements

Based on the Rayleigh model, the lateral D and longitudinal L dimensions of the focused laser beam spot are limited by diffraction and are calculated from Equations 8 and 9:

$$D = \frac{1.22\lambda}{NA}, \tag{8}$$

$$L = \frac{2\lambda n}{NA^2}; \tag{9}$$

where n – refractive index of the medium in which the beam is focused. For the fundamental radiation used in this assignment ($\lambda_f = 1030$ nm), an $NA = 1.4$ objective and the photopolymer ($n_f = 1.504$) this gives $D \approx 0.90$ µm and $L \approx 1.6$ µm.

We see that the dimensions of the focused laser beam can be reduced by using laser irradiation sources of shorter wavelengths or lenses with larger numerical apertures. In the first case, the choice of wavelength is limited by the combination of materials and laser sources suitable for multiphoton photopolymerization, and in the second case, the numerical aperture of the objective is limited by what the manufacturing technology allows.

Most practical applications of multiphoton polymerization arise precisely from the ability to form high (up to subdiffraction) spatial resolution 3D objects. The literature describes experiments in which the spatial resolution of 3DLL-formed structures is finer than 100 nm, an order of magnitude smaller than the wavelength of a typical femtosecond laser used in the 3DLL process [5]. Each photosensitive material has a characteristic polymerization threshold I_{pt}, above which a polymerization reaction is initiated. It is because of this threshold that the achievable structuring resolution may be better than the diffraction-limited value. In order to adapt the technology to new applications, it is particularly important to understand the fundamental limitations on the minimum size of any object segment (voxel).

Fig. 6 shows how the width of the polymerized region follows from the Gaussian intensity profile in the focal plane: only the part of the profile that lies above I_{pt} is polymerized, and only the part below I_{odt} survives undamaged. We see that the smallest possible segments (voxels) of polymerized material are formed when the exposing laser intensity only slightly exceeds the polymerization threshold; by controlling the intensity precisely, we can tune the lateral dimensions of the formed voxel [5].

There are several criteria that determine the fundamental resolution limits of 3DLL-fabricated structures. For all multiphoton processes, higher spatial resolution is achieved at a higher degree of nonlinearity of the process. If we consider a process with a specific degree of nonlinearity, in this case two-photon polymerization, the limit of the finest achievable resolution is determined by the

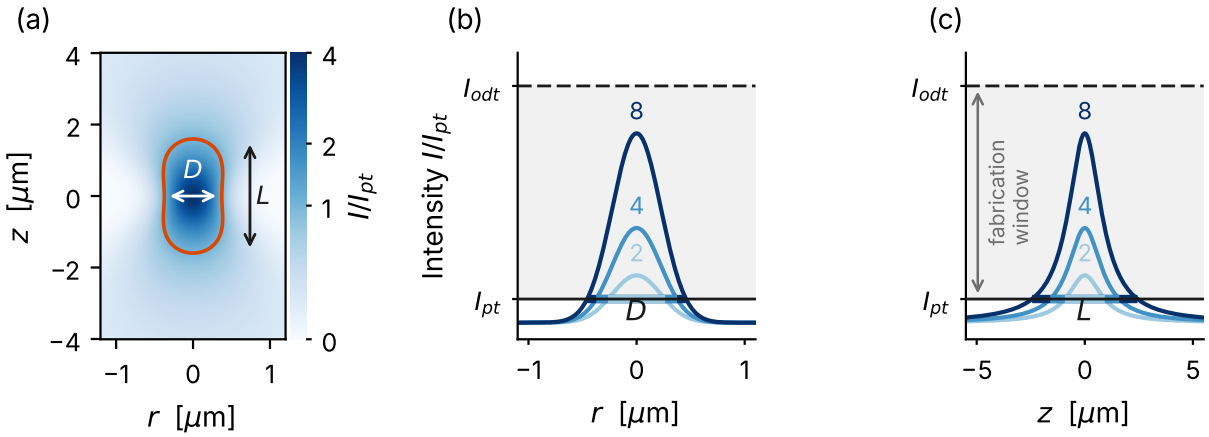


Fig. 6 Intensity distribution in the focus and the two thresholds, calculated for $\lambda_f = 1030$ nm, $NA = 1.4$ and $n = 1.5$ from the same Gaussian beam that Equations 11 and 12 assume. (a) Intensity in the r–z plane for a peak intensity $I_0 = 4I_{pt}$; the orange line is the $I = I_{pt}$ contour, which is the polymerized voxel, and D and L are its width and length. (b) Radial and (c) axial profiles through the focus for three peak intensities (in units of I_{pt}). Only the part of each profile above I_{pt} is polymerized – the thick bars on that line are D and L – and only the part below the optical damage threshold I_{odt} survives undamaged. A similar presentation of the two thresholds is given in [6].

smallest possible molecular structure of the specific material and by a factor indicating how close to the polymerization threshold one can work. Finally, the fundamental resolution limit is determined by the intensity distribution in the laser beam waist, which depends on the wavelength of the radiation and the *NA* of the focusing objective. Thus, both the structural properties of the material and the properties of the exposing beam determine the resolution of the multiphoton polymerization process [5].

To estimate the size of the polymerized volume (a volumetric pixel, or voxel), we will use the polymerization threshold parameter. We will assume that a photosensitive material is polymerized when a certain characteristic density of initiator molecules is activated – ρ_{th}. The density of activated initiator molecules $\rho(r,t)$ is expressed by Equation 10 [7]:

$$\frac{\partial \rho(r,t)}{\partial t} = (\rho_0 - \rho(r,t))\sigma_2 N^2(r,t); \tag{10}$$

where σ_2 – effective cross-section of two-photon initiator molecule activation, N – photon flux, $\rho_0(r,t)$ – initial density of initiator molecules. Approximating the light distribution in the focal plane ($z = 0$) with a Gaussian beam: $N(r,t) = N_0(t)\exp(-2r^2/r_0^2)$, assuming that the photon flux $N_0(t) = N_0$ is constant over the entire duration of the laser pulse, and neglecting the decrease in initiator between individual laser pulses, we can estimate the voxel width D, formed in the two-photon polymerization mode when the condition $\rho \geq \rho_{th}$ is satisfied:

$$D(N_0,t) = r_0\sqrt{\ln(\frac{\sigma_2 N_0^2 N_p \tau_L}{C})}, \tag{11}$$

$$C = \ln\left(\frac{\rho_0}{\rho_0 - \rho_{th}}\right)$$

where $N_p = ft$ – number of pulses delivered to one point of the material, f – pulse repetition rate, t – exposure duration of that point, τ_L – single laser pulse duration. Note that D is the voxel *width* (diameter), not a radius: the polymerized region extends to half of D on either side of the axis.

Similarly, for the axial light distribution at $r = 0$, where the Gaussian beam is given by $N(z) = N_0/(1 + z^2/z_R^2)$, the voxel length L can be calculated as:

$$L(N_0, t) = 2z_R\sqrt{\sqrt{\frac{\sigma_2 N_0^2 N_p \tau_L}{C}} - 1} \tag{12}$$

where $z_R = \pi r_0^2 n/\lambda$ – Rayleigh length.

Both expressions contain the same group $x = \sigma_2 N_0^2 N_p \tau_L / C$ and both vanish when $x = 1$: that condition is the polymerization threshold itself. The photon flux is proportional to the intensity ($I = h\nu N_0$) and x grows as N_0^2, so at a fixed number of pulses $x = (I/I_{pt})^2$ and the two equations depend on the single relative quantity I/I_{pt}. The square is a consequence of the two-photon nature of the absorption.

The same group also predicts how the voxel depends on the translation velocity, which is the second dependence measured in this assignment. A point of the material stays in the focal spot for a time $t \approx D/v$, so the number of pulses it receives is $N_p = ft \approx fD/v$, and x is inversely proportional to the velocity. Writing v_{pt} for the velocity at which the exposure just reaches the threshold at a given intensity, $x = v_{pt}/v$ and

$$D = r_0\sqrt{\ln\frac{v_{pt}}{v}}, \qquad L = 2z_R\sqrt{\sqrt{\frac{v_{pt}}{v}} - 1}. \tag{13}$$

The lateral dimension therefore depends on the velocity only logarithmically, which is a very weak dependence: reducing the velocity tenfold widens the voxel by a factor of less than two. The longitudinal dimension is more sensitive – far above the threshold $L \propto v^{-1/4}$ – so the aspect ratio L/D grows as the sample is translated more slowly. This is worth keeping in mind when the measured velocity dependence is compared with the model.

To form a voxel whose shape is as close to spherical as the model allows, it is necessary to use low laser pulse energy and short exposure time, in other words, work close to the polymerization threshold. Note, however, that a spherical voxel ($L/D = 1$) is not attainable in this model: even at the threshold $L/D \to 1.22\pi n/(NA\sqrt{2})$, which is about 2.9 for $NA = 1.4$ and $n = 1.5$. Working near the threshold ensures the highest possible polymerization resolution and the least elongated polymerized segment [5].

The dependences of the lateral and longitudinal dimensions of the voxel on the intensity of the laser beam used were calculated from Equations 11 and 12 ($NA = 1.4$ objective) and depicted graphically (Fig. 7 (a)). This model does not take into account any response or polymerization kinetics of

the polymerizable material, but it is suitable for the qualitative evaluation of the dimensional change of the voxel formed by the 3DLL method. We see that as the exposure intensity increases, the longitudinal dimension of the voxel increases faster than the lateral one. The dependence of the voxel aspect ratio L/D on the exposure intensity for focusing objectives with different numerical apertures is shown in Fig. 7 (b). It is noteworthy that the use of objectives with larger numerical apertures not only achieves a higher resolution in the lateral coordinates, but also lower values of the voxel length-to-width ratios.

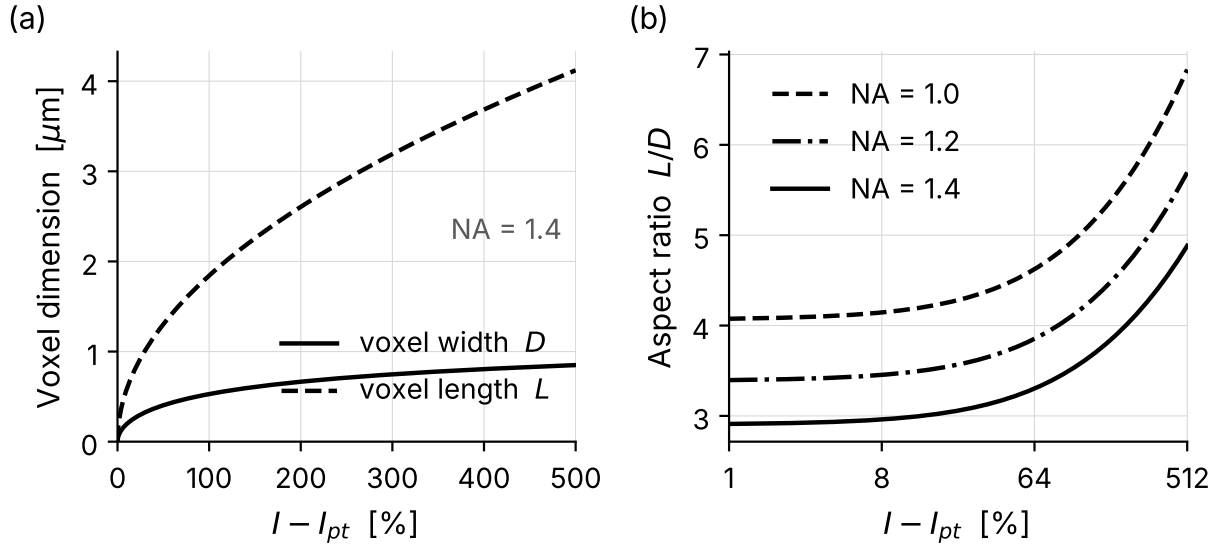


Fig. 7 Voxel dimensions calculated from Equations 11 and 12: (a) voxel width D and length L for an $NA = 1.4$ objective; (b) the length-to-width ratio L/D for objectives of different numerical aperture. Both equations vanish at the polymerization threshold, so the exposure is given as the relative intensity above it. Plotted for the fundamental wavelength $\lambda_f = 1030$ nm and photopolymer refractive index $n = 1.5$, with $r_0 = 0.61\lambda/NA$ and $z_R = \pi r_0^2 n/\lambda$.

Still, although such a theoretical model reflects the general trends in the resolution of the formed voxels well, the calculated values differ from those obtained experimentally. In contrast to the processing of materials by laser ablation, modeling the interaction of multiphoton polymerization requires not only the size of the spot into which the laser beam is focused, but also the exact three-dimensional distribution of the laser beam in the focal plane [7]. By deriving the equations describing the theoretical dimensions of the formed voxel, we simplified the analysis by approximating the energy distribution by the Gaussian beam. In addition, we completely ignored the irradiation response of the polymerizable material. In the formation of 3D objects in a real multiphoton polymerization system, the polymerization is initiated by long pulse bursts, and due to the translation of the sample in 3D space, the number of pulses acting on each unit of volume and their overlap are not constant. For this reason, an analytical description of the energy flow is essentially impossible. In addition, the finite energy stability of the laser pulses needs to be considered in a real 3DLL experiment [7].

Empirical methods are widely used in experimental work to determine the optimal processing

conditions. The lateral and longitudinal resolution of the formation of three-dimensional microstructures can be estimated based on two models: „resolution bridges“ [8] and „isolated voxels“ [9]. In both cases, the resolution is assessed by measuring the length and width of the voxel from images taken by a SEM.

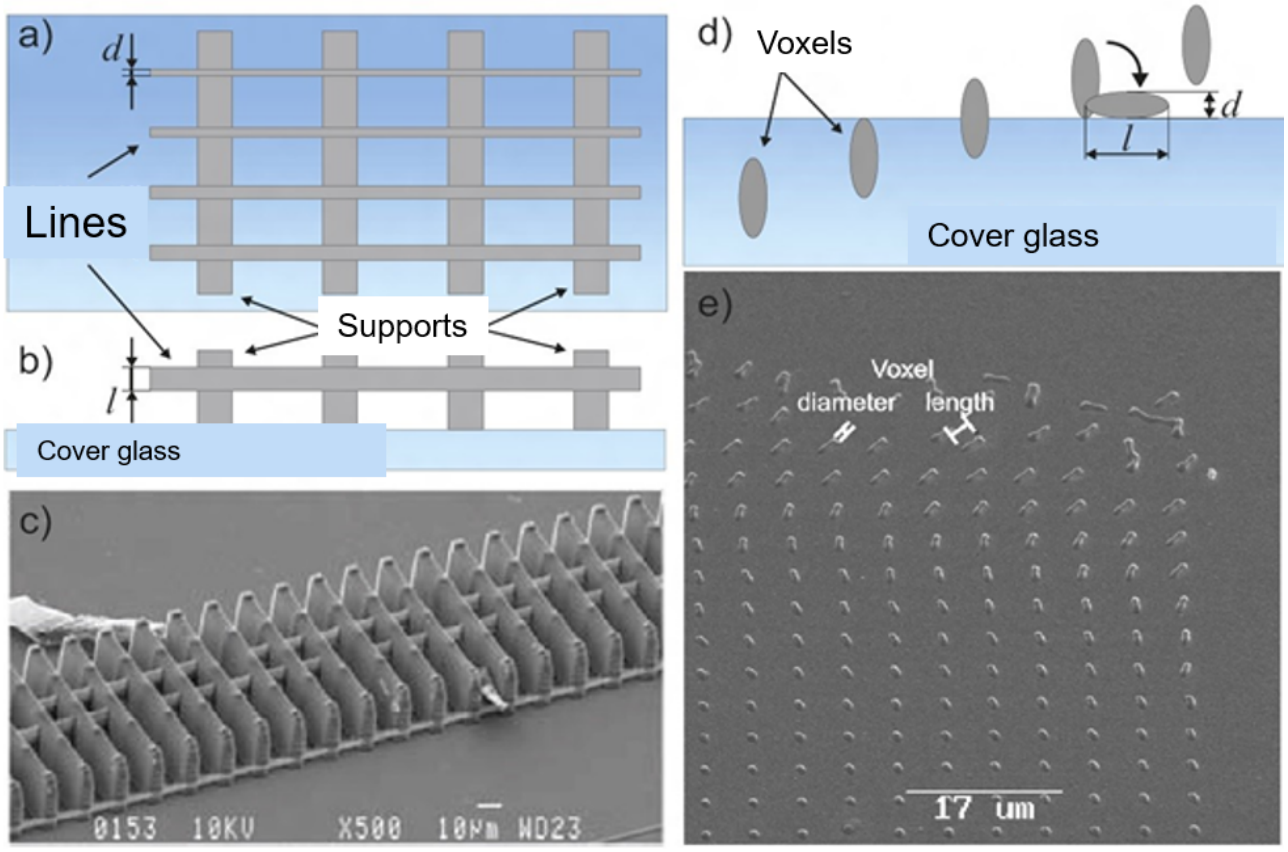


Fig. 8 Evaluation of the voxel lateral (D) and longitudinal (L) dimensions: (a) top view of „resolution bridges“ and (b) side view; (c) SEM image of produced „resolution bridges“ [8]; (d) side view of „isolated voxels“, adapted from [9]; (e) SEM image of an array of „isolated voxels“.

Based on the „resolution bridges“ model, the resolution is estimated by measuring the height and width of the lines. These lines are formed in a single pass between the supportive walls, which prevents the lines from collapsing and floating away during development, but allows the lines to avoid contact with the cover glass (Fig. 8 (a)–(c)). In order to evaluate the formation resolution as accurately as possible, the length of the lines must be ∼100 µm and they must be measured in their central part. This avoids errors caused by the acceleration and deceleration of the sample positioning system. Depending on which relationship is being investigated, a different laser irradiation intensity or sample translation velocity is selected for each line. As an alternative to the „resolution bridges“ method, the „isolated voxels“ method can be used. With this method, individual lines are no longer measured, but voxels. They are formed by sharply focusing the laser radiation into the volume of the photopolymer and changing the position of the focal plane of the objective relative to the cover glass. During this

voxel formation process, some voxels are formed in a photopolymer volume (when the laser radiation is focused too far from the cover glass), some in contact with the cover glass (focusing near the surface), and some voxel tips are cut off (focusing on the cover glass), Fig. 8 (d). The voxels formed in the volume of the photopolymer do not adhere to the cover glass and are therefore washed away during the development of the sample. Voxels that are in contact with the cover glass turn onto their side during development and adhere to the surface. It is these voxels that are measured to assess the formation resolution. For unambiguous evaluation of the formation resolution, the exposure duration of each voxel must be the same. If truncated voxels are measured, errors may occur because it is not ensured that at least half of the voxel protrudes above the surface. Based on the „isolated voxels“ method, it is possible to estimate not only the formation resolution, but also the shape of the voxel, which is not possible with the „resolution bridges“ method. However, this method is not suitable for investigating the dependence of the formation resolution on the sample translation velocity and for estimating the lateral resolution when it is less than 100 nm. It has been observed that individual voxels of such dimensions do not adhere to the surface and are washed away during development.

6.4 Scanning electron microscopy

In a SEM the image is not projected at once, as in an optical microscope, but built point by point. Electrons emitted by the gun are accelerated through a potential difference of typically 1–30 kV, focused by a system of magnetic lenses into a probe of a few nanometres in diameter and scanned in a raster across the surface of the sample. At every point of the raster the signal registered by the detector sets the brightness of the corresponding pixel of the image. The de Broglie wavelength of a 15 keV electron is about 0.01 nm, roughly five orders of magnitude shorter than the wavelength of visible light, so the resolution of the instrument is not limited by diffraction: it is limited by the diameter of the electron probe and by the size of the interaction volume in which the electrons are scattered within the sample, and in practice amounts to a few nanometres.

Two signals are used for imaging. Secondary electrons are knocked out of the atoms of the sample by the primary beam; their energies are low (below 50 eV), so only those generated in the topmost few nanometres escape. They therefore give a sharp, strongly topographic contrast, with edges and protrusions appearing bright. Backscattered electrons are primary electrons returned from the sample after elastic scattering; they retain a large part of their initial energy, emerge from a greater depth, and their yield grows with the atomic number of the material, so they give compositional contrast at a somewhat lower resolution. The tabletop microscope used in this assignment (TM-1000, *Hitachi*) operates at a fixed accelerating voltage of 15 kV, is equipped with a backscattered electron detector and covers a magnification range of 20× to 10 000×; the details are given in its manual.

The column and the chamber of the microscope are evacuated, and the sample must conduct the charge brought in by the beam. Dielectric samples – polymeric microstructures among them – accumulate this charge, which deflects the probe and produces bright streaks and a drifting image.

This is why the developed structures are sputter-coated with a 10–20 nm layer of silver or gold before the measurement (step 7 of the workflow): the metal film drains the charge to the sample holder and at the same time increases the electron yield. The thickness of the coating is a compromise: too thin a layer does not conduct, while too thick a one rounds off the sharp features of the structure and adds to the measured dimensions.

The depth of field of a SEM is far greater than that of an optical microscope of the same resolving power, because the electron probe converges at a very small angle. That is what makes it possible to image a tall, tilted structure at all. It is not unlimited, however: it falls roughly in inverse proportion to the magnification, so at the magnifications needed to measure a submicrometre line only a few micrometres of depth are sharp at once – less than the height of a „resolution bridge“. The microscope therefore has to be refocused on the part of the structure that is being measured, and every measurement must be taken where that feature itself is in focus. The lateral dimension D is measured directly in the top view. The longitudinal dimension L is measured in the tilted view, where it is foreshortened: the apparent length in the image is $L\sin\alpha$, α being the tilt angle away from the top view, so at the 45° tilt used in this assignment the measured value must be multiplied by $\sqrt{2}$. A detailed description of the construction of the microscope and of the formation of the image can be found in [10].

6.5 Materials used in multiphoton polymerization applications

In the most general case, photosensitive materials that can be structured by the multiphoton polymerization method are divided into two subgroups: positive and negative photoresists. The main difference between the structuring mechanisms of these materials is that, in the case of negative photoresists, the cross-linking of polymer chains is initiated in the light-exposed regions, while the monomers in the regions unaffected by the light are removed during development. In the case of positive photoresists the opposite occurs – exposure to light causes the polymer chains to break into smaller structural units, which are washed out during the development process [5]. Negative photoresists are most commonly used for the fabrication of functional 3D structures by direct laser writing. Additive manufacturing from negative photoresists makes it possible to produce structures of more varied and more complex shapes. On the other hand, positive photoresists are particularly well suited to the fabrication of embedded microfluidic components such as cavities and channels [5].

Modern photopolymers consist of a mixture of monomer / oligomer molecules doped with a photoinitiator. A considerable number of different types of materials are commercially available, and they are widely studied and applied for the fabrication of 3D nanostructures for various purposes. One such group of materials are the solid, epoxy-based materials SU8 [11] and CAR44 [5]. Both of these materials are widely applied for the fabrication of templates and three-dimensional microstructures by the multiphoton polymerization method. Another important subclass of negative photoresists are the liquid photopolymers – various acrylates and hybrid organic-inorganic photopolymers [5].

Hydrogels

As a possible alternative to structures produced from commercially available photopolymers, various hydrogels are widely examined in the scientific literature. Hydrogels are three-dimensional networks of polymer chains that swell in water while retaining their shape [12]. It has been established that hydrogels have a particularly high biocompatibility with living organisms and, in addition, exhibit hydration properties and a flexibility resembling that of natural organic tissue.

One of the most widely studied hydrogel-forming materials is poly(ethylene glycol) (PEG). PEG has been shown to have a particularly low cytotoxicity and for this reason it is widely used as a dispersant in the composition of many hygiene products (toothpaste, creams, shampoos) [1]. In addition, poly(ethylene glycol) molecules can be functionalized with acrylate groups, thereby increasing the photosensitivity of the monomers and creating an organic photopolymer suitable for structuring by the multiphoton polymerization method [1]. Materials based on poly(ethylene glycol) diacrylate are considered particularly suitable for implantation into and injection into living organisms because of their very low toxicity and immunogenicity.

Hybrid organic-inorganic polymers

Another group of materials important for 3DLL applications is „Ormosil“ (*organically modified silica*). The polymer precursor SZ2080, which belongs to this group of materials, is increasingly used for the fabrication of structures for micro-optics, regenerative medicine, optoelectronics and photonics [13]. The inorganic backbone of the polymer precursor consists of a –Si–O–Zr–O network, to which polymerizable methacrylate branches are attached. The polymer precursor is attractive because of the possibility of tuning the refractive index by changing the ratio of the organic and inorganic parts, its optical transparency in the 400–2700 nm wavelength range and its low shrinkage [14], as well as its good biocompatibility.

Because of its semi-solid, glassy state once the solvent has been evaporated, the SZ2080 polymer precursor is convenient for experimentation, both because of the freedom of the laser writing algorithm and because of the simpler transport, storage and repeated characterization of the samples.

References

[1] M. Malinauskas, *Fabrication of Functional 3D Micro/Nanostructures by Laser Multiphoton Polymerization Technique*, Ph.D. thesis, Vilniaus Universitetas (2010).

[2] G. Odian, *Principles of Polymerization* (John Wiley & Sons, Hoboken, New Jersey, 2004), 4th edition.

[3] F. Jipa, M. Zamfirescu, A. Velea, M. Popescu, R. Dabu, Femtosecond laser lithography in organic and non-organic materials, in *Updates in Advanced Lithography* (InTech, 2013), chapter 3, 65–94.

[4] A. Ovsianikov, M. Gruene, M. Pflaum, L. Koch, F. Maiorana, M. Wilhelmi, A. Haverich, B. Chichkov, Laser printing of cells into 3D scaffolds, Biofabrication **2**(1), 014104 (2010).

[5] A. Ovsianikov, S. Passinger, R. Houbertz, B. N. Chichkov, *Three Dimensional Material Processing with Femtosecond Lasers* (Springer US, 2007), pp. 121–157.

[6] E. Skliutas, G. Merkininkaitė, S. Maruo, W. Zhang, W. Chen, W. Deng, J. Greer, G. von Freymann, M. Malinauskas, Multiphoton 3D lithography, Nat. Rev. Methods Primers **5**, 15 (2025).

[7] J. Serbin, A. Egbert, A. Ostendorf, B. N. Chichkov, R. Houbertz, G. Domann, J. Schulz, C. Cronauer, L. Fröhlich, M. Popall, Femtosecond laser-induced two-photon polymerization of inorganic–organic hybrid materials for applications in photonics, Opt. Lett. **28**(5), 301 (2003).

[8] R. J. DeVoe, H. Kalweit, C. A. Leatherdale, T. R. Williams, Voxel shapes in two-photon microfabrication, in K. D. Belfield, S. J. Caracci, F. Kajzar, C. M. Lawson, A. T. Yeates (eds.), *Multiphoton Absorption and Nonlinear Transmission Processes: Materials, Theory, and Applications* (SPIE, 2003), volume 4797, 310–316.

[9] H. B. Sun, T. Tanaka, S. Kawata, Three-dimensional focal spots related to two-photon excitation, Appl. Phys. Lett. **80**(20), 3673–3675 (2002).

[10] J. I. Goldstein, D. E. Newbury, J. R. Michael, N. W. M. Ritchie, J. H. J. Scott, D. C. Joy, *Scanning Electron Microscopy and X-Ray Microanalysis* (Springer, New York, 2018), 4th edition.

[11] S. Juodkazis, V. Mizeikis, K. K. Seet, M. Miwa, H. Misawa, Two-photon lithography of nanorods in SU-8 photoresist, Nanotechnology **16**(6), 846–849 (2005).

[12] M. Bae, R. A. Gemeinhart, R. Divan, K. J. Suthar, D. C. Mancini, Fabrication of poly(ethylene glycol) hydrogel structures for pharmaceutical applications using electron beam and optical lithography, J. Vac. Sci. Technol. B **28**(6), C6P24–C6P29 (2010).

[13] A. Žukauskas, *Optinių elementų šviesos valdymui mikrometriniame mastelyje formavimas tiesioginio lazerinio rašymo būdu*, Ph.D. thesis, Vilniaus universitetas ir Fizinių ir technologijos mokslų centras (2015).

[14] A. Ovsianikov, J. Viertl, B. Chichkov, M. Oubaha, B. MacCraith, I. Sakellari, A. Giakoumaki, D. Gray, M. Vamvakaki, M. Farsari, C. Fotakis, Ultra-low shrinkage hybrid photosensitive material for two-photon polymerization microfabrication, ACS Nano **2**(11), 2257–2262 (2008).